

Noncritical phasematching behavior in thin-film lithium niobate frequency converters

PAULINA S. KUO* 

Information Technology Laboratory, National Institute of Standards and Technology, 100 Bureau Drive, Gaithersburg, Maryland 20899, USA

*Corresponding author: paulina.kuo@nist.gov

Received 30 September 2021; revised 28 November 2021; accepted 29 November 2021; posted 1 December 2021; published 17 December 2021

We present a study of noncritical phasematching behavior in thin-film, periodically poled lithium niobate (PPLN) waveguides. Noncritical phasematching refers to designing waveguides so that the phasematching is insensitive to variations in waveguide thickness, width, or other parameters. For waveguide thickness (the dimension with greatest nonuniformity due to fabrication), we found that phasematching sensitivity can be minimized but not eliminated. We estimate limits on the acceptable thickness variation and discuss scaling with device length for second-harmonic generation and sum-frequency generation in thin-film PPLN frequency converters.

<https://doi.org/10.1364/OL.444846>

There is increasing interest in thin-film lithium niobate (LN) for electro-optic modulation [1], integrated photonics [2,3], and optical frequency conversion. There have been numerous demonstrations of nonlinear optical frequency conversion in thin-film LN, including second-harmonic generation (SHG) in waveguides [4–11] and in resonator structures [12–14], supercontinuum generation [15], spontaneous parametric down-conversion [12,16,17], and optical parametric oscillation [18]. Thin-film LN waveguides offer tight optical confinement for ultra-high conversion efficiencies, estimated to be 20 times higher than state-of-the-art diffused waveguides [7]. The waveguides also allow dispersion engineering for ultra-broad bandwidth conversion [15]. Combined with the electro-optic modulation capabilities of LN, the thin-film LN platform offers great promise for integrating together photon-pair sources, quantum information processing [19], and quantum frequency conversion [20].

Phasematching is required for efficient optical frequency conversion [21]. Earlier thin-film LN waveguide devices employed waveguide dispersion and intermodal mixing to achieve phasematching [5,6,12]. More recently, periodic poling of thin-film LN [7–11,13–17] to achieve quasi-phasematching (QPM) [22] has enabled flexibility in choosing operating wavelengths and waveguide cross-sections while also accessing the lowest-order spatial modes for better modal overlap. The waveguide geometry has a significant effect on the total dispersion, which affects phasematching. By using QPM, the choice of waveguide cross section is no longer tightly coupled to the phasematching wavelength. Instead, the thin-film LN frequency converter can be

designed by first determining the effective refractive indices for the interacting spatial modes and wavelengths, then calculating the phase mismatch ($\Delta\beta$) and the required QPM period ($\Lambda_{\text{QPM}} = 2\pi/\Delta\beta$).

The optical properties of the waveguides are sensitive to fabrication imperfections, which in turn affect the phasematching. Variations in waveguide width, height, etch depth and other parameters can change the local effective index. Nonuniform effective indices lead to nonuniform phasematching, which is manifested in shifted or distorted tuning curves, and may limit the conversion efficiency. It is desirable to design waveguides to achieve noncritical phasematching [23–25], where the phasematching is to first order independent of the waveguide width or other geometric parameter. Noncritical phasematching will be particularly important in long waveguides, such as those needed in quantum frequency conversion to achieve near 100% conversion efficiency [26]. Although some initial considerations [17,27] have been given to identifying waveguide geometries that are more tolerant to fabrication variations, to the best of the author's knowledge, a systemic study of noncritical phasematching has not been performed for thin-film periodically poled lithium niobate (PPLN) waveguides. Here, we present such a study.

Let us first consider SHG. For SHG in a QPM grating with period Λ_{QPM} , the fundamental and second-harmonic (SH) waves (at frequencies ω_1 and ω_2 , respectively) should satisfy

$$\begin{aligned}\omega_2 &= 2\omega_1 \\ \Delta\beta - 2\pi/\Lambda_{\text{QPM}} &= 0 \\ \Delta\beta &= \beta_2 - 2\beta_1\end{aligned}\quad (1)$$

where β_i is the propagation constant ($\beta_i = \omega_i n_{\text{eff},i}/c$), c is the speed of light, and $n_{\text{eff},i}$ is the effective refractive index. Here Λ_{QPM} is fixed during fabrication, but there may be variations in $\Delta\beta$ due to nonuniformity of the waveguide. The parameter $\Delta\beta$ depends on geometrical parameters of the waveguide, which we can label f_m where f_m could represent the waveguide width, etch depth, etc. Here f_m could change along the length of the device due to fabrication imperfections leading to changes in $\Delta\beta$. Assuming f_m only varies a small amount δf_m around $f_{m,0}$, we can write

$$\Delta\beta(f_m) = \Delta\beta(f_{m,0}) + \frac{\partial\Delta\beta}{\partial f_m} \delta f_m + O((\delta f_m)^2). \quad (2)$$

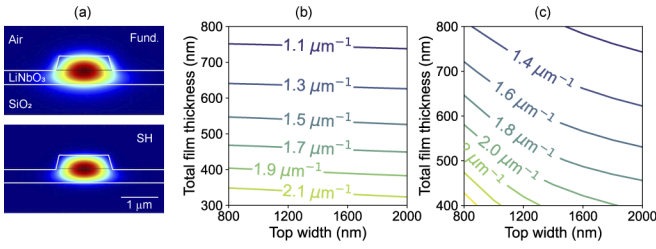


Fig. 1. (a) Calculated fundamental and SH TE modes in an x -cut PPLN waveguide; and $\Delta\beta$ for different waveguide widths and thicknesses with etch depth set to (b) 50 nm and (c) 350 nm.

If $\partial\Delta\beta/\partial f_m = 0$, then the phasematching is considered “non-critical” in the parameter f_m , meaning that phasematching is to first order independent of f_m [23]. It is desirable to identify waveguide geometries that achieve noncritical phasematching, particularly for the geometrical parameter that has largest variation. If noncritical phasematching is not possible, then we can choose geometries that minimize $|\partial\Delta\beta/\partial f_m|$.

In this work, we examine PPLN waveguides made from both x -cut and z -cut LN wafers. For x -cut PPLN waveguides, the poling direction and the optical polarizations needed to access LN’s large $d_{33} = d_{zzz}$ coefficient lie in the plane of the wafer, whereas for z -cut waveguides, they are normal to the wafer plane. That is, x -cut and z -cut PPLN waveguides utilize the transverse electric (TE) and transverse magnetic (TM) polarizations, respectively. Generally speaking, it is easier to fabricate x -cut PPLN waveguides because the poling electrodes can be placed adjacent to the waveguides rather than directly on top of the z -cut waveguides (where the poling electrodes need to be removed later in order to perform optical experiments [14]).

We used COMSOL to simulate light propagating in thin-film LN waveguides. We modeled MgO-doped LN [28] thin films sitting on a 2- μm -thick SiO_2 layer. We varied the total LN film thickness, etch depth and waveguide top width. For the x -cut PPLN waveguides, the sidewall angle was taken to be 75° [17] and for z -cut waveguides, the sidewall angle was 62° [11,14]. We examined SHG with 1570 nm fundamental wavelength and calculated the effective indices and $\Delta\beta$ for different waveguide geometries. From $\Delta\beta$, the required QPM period can be calculated.

Figure 1(a) shows the calculated fundamental and SH TE modes for an example x -cut waveguide. Figures 1(b) and 1(c) are contour plots of $\Delta\beta$ for x -cut PPLN waveguides as a function of top waveguide width and total LN film thickness with etch depth of 50 and 350 nm, respectively. Contour lines that are perfectly horizontal or vertical represent waveguide geometries that are noncritically phasematched in waveguide width or in LN film thickness, respectively. We see that for the 50-nm etched waveguides (Fig. 1(b)), the contours are nearly horizontal, which means that the phasematching is quite insensitive to waveguide width. However, for the 350-nm-deep etch, there is more curvature in the contours with $|\partial\Delta\beta/\partial w|$ decreasing at larger widths, w .

In thin-film LN devices, the largest source of dimensional uncertainty is typically the LN film thickness. This thickness nonuniformity can be 40 nm [29], whereas the waveguide width (using e-beam lithography) and etch depth are typically controlled with higher precision. Assuming uniform etching, any variation in the total LN film thickness is transferred into waveguide height variations. In Fig. 2(a), we fix the waveguide top

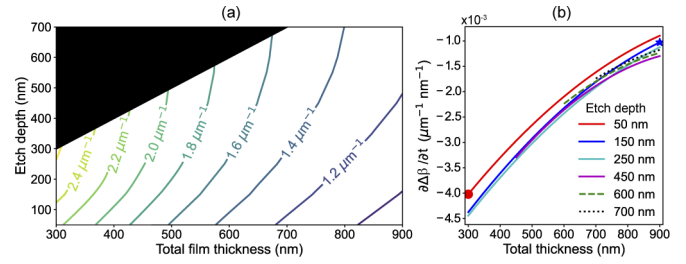


Fig. 2. (a) Dependence of $\Delta\beta$ on etch depth and total film thickness for a 1200-nm-wide x -cut waveguide. (b) Calculated slopes $\partial\Delta\beta/\partial t$.

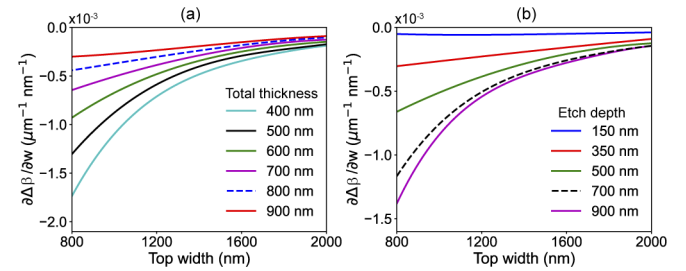


Fig. 3. Slopes $\partial\Delta\beta/\partial w$ for x -cut waveguides with (a) etch depth fixed to 350 nm and (b) total thickness fixed to 900 nm.

width to 1200 nm and calculate $\Delta\beta$ as a function of etch depth and total LN film thickness. Plots at other waveguide widths are qualitatively similar. The black region represents structures that are not physically possible. Our calculations did not show any geometries having horizontal contours where $\partial\Delta\beta/\partial t \approx 0$. Therefore, one tries to minimize the dependence of the phasematching on film thickness, t . That is, because $\partial\Delta\beta/\partial t \neq 0$, we wish to minimize $|\partial\Delta\beta/\partial t|$. Figure 2(b) plots the slopes $\partial\Delta\beta/\partial t$ for different LN thicknesses and etch depths. The slopes are calculated using a polynomial fit to the data and using the fitted polynomial to calculate the derivatives. For all etch depths, we see that $|\partial\Delta\beta/\partial t|$ is smaller for larger LN film thicknesses. For 900 nm thickness, $|\partial\Delta\beta/\partial t| \approx 1 \times 10^{-3} \mu\text{m}^{-1} \text{nm}^{-1}$. In comparison, the sensitivity to waveguide width shown in Fig. 1(b) is $|\partial\Delta\beta/\partial w| \approx 5 \times 10^{-5} \mu\text{m}^{-1} \text{nm}^{-1}$.

For completeness, we also calculated $\partial\Delta\beta/\partial w$, the sensitivity to waveguide width. In Fig. 3(a), we show $\partial\Delta\beta/\partial w$ for waveguides with etch depth fixed to 350 nm (same data as Fig. 1(c)). In Fig. 3(b), we plot $\partial\Delta\beta/\partial w$ for waveguides with total film thickness fixed to 900 nm. For the 150 nm etch depth (blue curve in Fig. 3(b)), $|\partial\Delta\beta/\partial w| \approx 5 \times 10^{-5} \mu\text{m}^{-1} \text{nm}^{-1}$, which was nearly constant over the range of widths studied. We note that the red curves in these two plots represent the same geometries.

One might ask how the sensitivity $\partial\Delta\beta/\partial t$ (or $\partial\Delta\beta/\partial w$) translates to distortions in the SHG tuning curve. Following theory outlined in [22], the SH electric field, E_2 , in a QPM grating grows as

$$\frac{dE_2}{dz} = \Gamma d_{\text{eff}} \exp(-i\Delta\beta'z), \quad (3)$$

where $\Gamma = i\omega_1 E_1^2/n_{\text{eff},2}c$, $d_{\text{eff}} = 2d/\pi$ is the effective nonlinearity for QPM interactions, d is the nonlinear coefficient, $\Delta\beta' = \Delta\beta - K_{\text{QPM}}$, and $K_{\text{QPM}} = 2\pi/\Lambda_{\text{QPM}}$. For constant $\Delta\beta'$, Eq. (3) can be integrated over the device length, L , to obtain

$$E_2(L) = \Gamma d_{\text{eff}} L \exp(-i\Delta\beta'L/2) \text{sinc}(\Delta\beta'L/2). \quad (4)$$

A simple model of position-dependent phase mismatch is

$$\Delta\beta'(z) = \Delta\beta_0 + \alpha z - K_{\text{QPM}} = \Delta\beta'_0 + \alpha z, \quad (5)$$

where the constant α is the chirp parameter, which we assume arises from a linear variation in t . If the difference in thickness between one end of the grating and the other is Δt , then

$$\alpha = \frac{\partial\Delta\beta}{\partial t} \frac{\Delta t}{L}. \quad (6)$$

Inserting Eq. (5) into Eq. (3) and integrating, we obtain

$$\begin{aligned} E_2(L) &= \Gamma d_{\text{eff}} (F(L) - F(0)) \\ F(z) &= A_0 \text{Erfi} \left(\frac{(-1)^{3/4} (\Delta\beta'_0 + 2\alpha z)}{2\sqrt{\alpha}} \right) \\ A_0 &= \frac{-(-1)^{1/4} \sqrt{\pi} \exp(i\Delta\beta'_0/4\alpha)}{2\sqrt{\alpha}} \end{aligned} \quad (7)$$

where $\text{Erfi}(x) = -i\text{Erf}(ix)$ and $\text{Erf}(x)$ is the error function. Numerically, we found that Eq. (7) reproduces Eq. (4) for $\alpha L^2 \lesssim 0.1$ and showed distorted curves for $\alpha L^2 > 0.1$. However, for very small αL^2 ($< 10^{-6}$), Eq. (7) deviates from the expected sinc² curves, which may be due to numerical errors in our computation.

Using this model of the effect of linearly varying LN film thickness, we can calculate the SHG tuning curves. In Fig. 4, we plot SH intensity, $|E_2(L)|^2$, for the ideal waveguide (Eq. (4)) and the waveguide with nonuniform thickness (Eq. (7)). We set $|\Gamma d_{\text{eff}} L| = 1$ and the length to 5 mm. We compare the ideal cases to waveguides having different amounts of thickness variation Δt . We examined two waveguide geometries: (a) 300 nm total thickness, 50 nm etch depth, and 1240 nm top width (Ref. [17]), and (b) 900 nm total thickness, 150 nm etch depth, and 1200 nm top width, which are marked in Fig. 2(b) by the red circle and blue star, respectively. The calculations show that small $|\alpha|$ values shift the tuning curve (to shorter wavelengths for $\alpha < 0$ shown here because $\partial\Delta\beta/\partial t < 0$, and to longer wavelengths for $\alpha > 0$). Larger $|\alpha|$ values produce larger shifts, decrease the maximum conversion efficiency, and distort and broaden the tuning curve. The red curves in Fig. 4 represent devices where the peak intensity is half of the ideal value. For the 300- and 900-nm-thick waveguides, Δt that produces the red curves are 0.54 and 2.2 nm, respectively. These values of Δt represent estimates of the acceptable thickness variation. Note that this model also gives the equivalent change in effective QPM period. Taking the example in Fig. 4(b), the designed QPM period is $2\pi/\Delta\beta_0 = 6.331 \mu\text{m}$, and $\Delta t = 2.2 \text{ nm}$ results in $\Delta\beta = \Delta\beta_0 + (\partial\Delta\beta/\partial t)\Delta t = 2\pi/6.345 \mu\text{m}^{-1}$, a 14-nm change in effective QPM period.

The amount of distortion to the SHG tuning curves is governed by the dimensionless quantity αL^2 where

$$\alpha L^2 = \frac{\partial\Delta\beta}{\partial t} \Delta t L. \quad (8)$$

For the red curves in Fig. 4, $\alpha L^2 = 11$. Equation (8) implies that the amount of allowed thickness variation scales as $1/L$ assuming αL^2 and $\partial\Delta\beta/\partial t$ are fixed. This scaling behavior agrees with analyses presented in [30]. We note for waveguides, the conversion efficiency scales as L^2 and the bandwidth scales as $1/L$.

We also examined SHG in z -cut PPLN waveguides. We found that thin z -cut waveguides ($\approx 300 \text{ nm}$ thickness) and those with

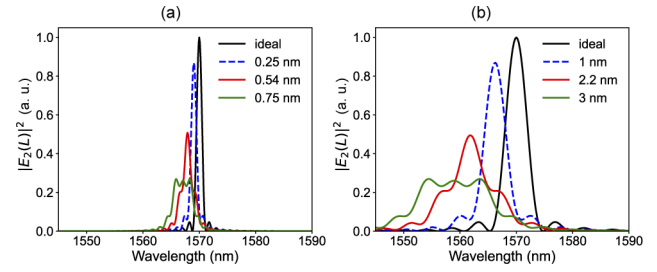


Fig. 4. SHG tuning curves in the presence of different amounts of Δt for 5-mm-long, x -cut PPLN waveguides with (a) 300 nm total thickness, 50 nm etch depth, and 1240 nm top width [17] and with (b) 900 nm total thickness, 150 nm etch depth, and 1200 nm top width.

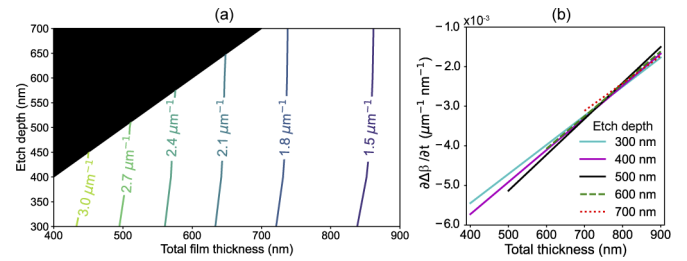


Fig. 5. (a) Dependence of $\Delta\beta$ on etch depth and total film thickness for a 1200-nm-wide z -cut waveguide. (b) Calculated slopes $\partial\Delta\beta/\partial t$.

more shallow etch depths ($< 200 \text{ nm}$) did not support TM waveguide modes. For geometries that do support TM modes, the dependence of phasematching on waveguide width was similar to that for moderately etched x -cut waveguides (Fig. 1(c)) where larger widths are associated with smaller $\Delta\beta$ and more horizontal contours (smaller $|\partial\Delta\beta/\partial w|$). Figure 5(a) plots the dependence of $\Delta\beta$ on etch depth and total LN film thickness for z -cut waveguides with the waveguide width fixed to 1200 nm. The sensitivity of phasematching to thickness, $\partial\Delta\beta/\partial t$, is shown in Fig. 5(b) where, similar to x -cut PPLN waveguides, larger LN thicknesses have lower sensitivity to thickness variations.

It is likely that the most demanding application for thin-film LN waveguides will be near 100% conversion efficiency sum-frequency generation (SFG) and difference-frequency generation needed for quantum frequency conversion. Achieving high absolute conversion efficiency will require long waveguide lengths and/or high pump powers. Longer waveguides will likely be more sensitive to fabrication imperfections. We examined SFG of $1550 \text{ nm} + 1900 \text{ nm} \rightarrow 854 \text{ nm}$ in x -cut thin-film PPLN waveguides. Figure 6(a) plots the dependence of $\Delta\beta$ for SFG on etch depth and total LN film thickness for 1200-nm-wide x -cut waveguides. Figure 6(b) shows the sensitivity to thickness, $\partial\Delta\beta/\partial t$. Using a geometry with low sensitivity to thickness, marked by the blue star in Fig. 6(a) having $|\partial\Delta\beta/\partial t| = 1 \times 10^{-3} \mu\text{m}^{-1} \text{ nm}^{-1}$, we calculated the distortion to the SFG tuning curves caused by a linearly varying thickness. We assumed the 1900-nm beam is fixed in wavelength and looked at the tuning near the 1550-nm signal. Here $|E_3(L)|^2$ is the intensity of the generated sum-frequency beam. These curves are calculated in the low conversion regime (in a similar fashion to Eqs. (4) and 7). The PPLN waveguide length is taken to be 5

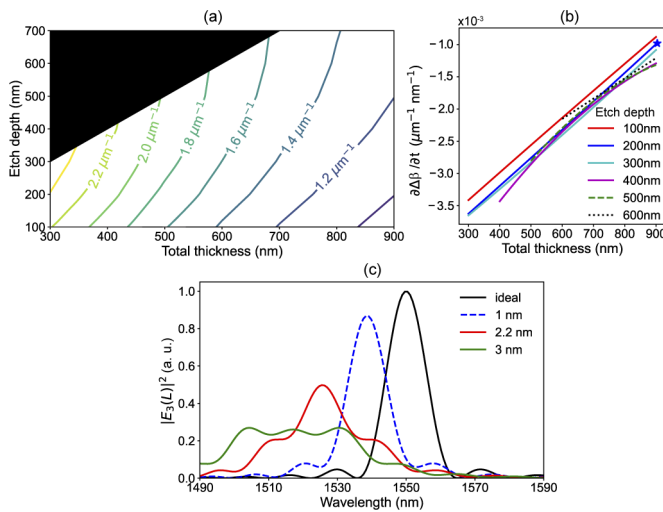


Fig. 6. (a) Dependence of $\Delta\beta$ for SFG on etch depth and total film thickness for an x -cut PPLN waveguide with 1200 nm top width and 5 mm length. (b) Calculated slopes $\partial\Delta\beta/\partial t$. (c) SFG tuning curve distortion caused by thickness variation for waveguides with 900 nm total thickness, 200 nm etch depth, and 1200 nm top width (indicated by blue star in (b)).

mm. The calculation shows that $\Delta t = 2.2$ nm will cause the SFG conversion efficiency to drop by half compared with the ideal case. Longer SFG devices will have tighter constraints on Δt ($\propto 1/L$).

In conclusion, we have presented a study of noncritical phase-matching behavior in thin-film, PPLN waveguides. Geometries exist where the sensitivity to waveguide width and etch depth are very low, but we found that the sensitivity to waveguide thickness (the dimension with highest variation due to fabrication) is nonzero for all the waveguide geometries studied (LN thicknesses between 300 and 900 nm, waveguide widths between 800 and 2000 nm, and etch depths between 50 nm and the full LN film thickness). Thicker waveguides have the lowest sensitivity to thickness variations. Etch depth has a smaller impact than thickness on $\partial\Delta\beta/\partial t$. To understand the effect of nonzero $\partial\Delta\beta/\partial t$, we calculated the output spectra assuming a linear chirp in the phase mismatch. We found that for devices with small thickness sensitivity ($|\partial\Delta\beta/\partial t| = 1 \times 10^{-3} \mu\text{m}^{-1}\text{nm}^{-1}$), SHG in a 5-mm-long device was reduced by 50% for a 2.2 nm variation in thickness. Waveguides with thicknesses greater than 900 nm will exhibit lower sensitivity of the phase-matching to thickness variations, but these are generally not commercially available. We did extend the numerical studies shown in Fig. 6(b) to thicker SFG devices and found that $\partial\Delta\beta/\partial t$ never reached zero; $|\partial\Delta\beta/\partial t|$ reached a minimum value of $4.5 \times 10^{-4} \mu\text{m}^{-1}\text{nm}^{-1}$ for 1.7 μm LN film thickness (with 600 nm etch depth and 1200 nm top width). This study highlights the importance in controlling the uniformity of the LN film thickness for producing high-quality frequency-conversion devices. One possible strategy to circumvent the tuning curve distortions caused by LN thickness variations will be to incorporate high- Q resonators, such as in Refs. [13,14]. The resonator can both enhance conversion efficiency and produce a sharply defined spectral response.

Disclosures. The author declares no conflicts of interest. Certain commercial equipment, materials or computational software are identified in this paper in order to specify device fabrication, the experimental procedure and data analysis adequately. Such identification is not intended to imply

endorsement by the National Institute of Standards and Technology, nor is it intended to imply that the equipment, material or software identified are necessarily the best available.

Data availability. Data underlying the results presented in this paper are not publicly available at this time but may be obtained from the author upon reasonable request.

REFERENCES

- C. Wang, M. Zhang, X. Chen, M. Bertrand, A. Shams-Ansari, S. Chandrasekhar, P. Winzer, and M. Lončar, *Nature* **562**, 101 (2018).
- M. Zhang, C. Wang, P. Kharel, D. Zhu, and M. Lončar, *Optica* **8**, 652 (2021).
- D. Zhu, L. Shao, M. Yu, R. Cheng, B. Desiatov, C. J. Xin, Y. Hu, J. Holzgrafe, S. Ghosh, A. Shams-Ansari, E. Puma, N. Sinclair, C. Reimer, M. Zhang, and M. Lončar, *Adv. Opt. Photonics* **13**, 242 (2021).
- L. Chang, Y. Li, N. Volet, L. Wang, J. Peters, and J. E. Bowers, *Optica* **3**, 531 (2016).
- C. Wang, X. Xiong, N. Andrade, V. Venkataraman, X.-F. Ren, G.-C. Guo, and M. Lončar, *Opt. Express* **25**, 6963 (2017).
- R. Luo, Y. He, H. Liang, M. Li, and Q. Lin, *Optica* **5**, 1006 (2018).
- C. Wang, C. Langrock, A. Marandi, M. Jankowski, M. Zhang, B. Desiatov, M. M. Fejer, and M. Lončar, *Optica* **5**, 1438 (2018).
- A. Rao, K. Abdelsalam, T. Sjaardema, A. Honardoost, G. F. Camacho-Gonzalez, and S. Fathpour, *Opt. Express* **27**, 25920 (2019).
- J.-Y. Chen, Y. M. Sua, Z.-H. Ma, C. Tang, Z. Li, and Y.-P. Huang, "Efficient parametric frequency conversions in lithium niobate nanophotonic chips," arXiv:1903.08722 (2019).
- J. Zhao, M. Rüsing, M. Roeper, L. M. Eng, and S. Mookherjee, *J. Appl. Phys.* **127**, 193104 (2020).
- J.-Y. Chen, C. Tang, Z.-H. Ma, Z. Li, Y. M. Sua, and Y.-P. Huang, *Opt. Lett.* **45**, 3789 (2020).
- R. Luo, H. Jiang, S. Rogers, H. Liang, Y. He, and Q. Lin, *Opt. Express* **25**, 24531 (2017).
- J.-Y. Chen, Z.-H. Ma, Y. M. Sua, Z. Li, C. Tang, and Y.-P. Huang, *Optica* **6**, 1244 (2019).
- J. Lu, J. B. Surya, X. Liu, A. W. Bruch, Z. Gong, Y. Xu, and H. X. Tang, *Optica* **6**, 1455 (2019).
- M. Jankowski, C. Langrock, B. Desiatov, A. Marandi, C. Wang, M. Zhang, C. R. Phillips, M. Lončar, and M. M. Fejer, *Optica* **7**, 40 (2020).
- B. S. Elkus, K. Abdelsalam, A. Rao, V. Velez, S. Fathpour, P. Kumar, and G. S. Kanter, *Opt. Express* **27**, 38521 (2019).
- J. Zhao, C. Ma, M. Rüsing, and S. Mookherjee, *Phys. Rev. Lett.* **124**, 163603 (2020).
- J. Lu, A. A. Sayem, Z. Gong, J. B. Surya, C.-L. Zou, and H. X. Tang, *Optica* **8**, 539 (2021).
- F. Flamini, N. Spagnolo, and F. Sciarrino, *Rep. Prog. Phys.* **82**, 016001 (2019).
- P. Kumar, *Opt. Lett.* **15**, 1476 (1990).
- R. W. Boyd, *Nonlinear Optics, Third Edition* (Academic Press, Amsterdam, 2008).
- M. Fejer, G. Magel, D. Jundt, and R. Byer, *IEEE J. Quantum Electron.* **28**, 2631 (1992).
- E. J. Lim, S. Matsumoto, and M. M. Fejer, *Appl. Phys. Lett.* **57**, 2294 (1990).
- K. R. Parameswaran, R. K. Route, J. R. Kurz, R. V. Roussev, M. M. Fejer, and M. Fujimura, *Opt. Lett.* **27**, 179 (2002).
- M. Santandrea, M. Stefszky, V. Ansari, and C. Silberhorn, *New J. Phys.* **21**, 033038 (2019).
- J. S. Pelc, L. Ma, C. R. Phillips, Q. Zhang, C. Langrock, O. Slattery, X. Tang, and M. M. Fejer, *Opt. Express* **19**, 21445 (2011).
- X.-H. Tian, W. Zhou, K.-Q. Ren, C. Zhang, X. Liu, G.-T. Xue, J.-C. Duan, X. Cai, X. Hu, Y.-X. Gong, Z. Xie, and S.-N. Zhu, *Chin. Opt. Lett.* **19**, 060015 (2021).
- O. Gayer, Z. Sacks, E. Galun, and A. Arie, *Appl. Phys. B* **91**, 343 (2008).
- NANOLN, private communication.
- M. Santandrea, M. Stefszky, and C. Silberhorn, *Opt. Lett.* **44**, 5398 (2019).